Temperature Dependence of Backbone Dynamics in Loops of Human Mitochondrial Heat Shock Protein 10†

Samuel J. Landry,*,‡ N. Kalaya Steede,‡ and Karol Maskos‡,§

Department of Biochemistry, Tulane University School of Medicine, New Orleans, Louisiana 70112, and Coordinated Instrumentation Facility, Tulane University, New Orleans, Louisiana 70118

Received May 15, 1997; Revised Manuscript Received June 27, 1997⊗

ABSTRACT: A highly flexible, yet conserved polypeptide loop of Hsp10 mediates binding to Hsp60 in the course of chaperonin-dependent protein folding. Previous transferred nuclear Overhauser effect (trNOE) studies with peptides based on the mobile loop of the *Escherichia coli* and bacteriophage T4 Hsp10s suggested that the mobile loop adopts a characteristic hairpin turn upon binding to the *E. coli* Hsp60 GroEL. In this paper, we identify the sequence and characterize the nascent structure and dynamics of the 18-residue mobile loop in the ^{15}N-enriched human Hsp10. We also identify four residues of another flexible loop, the roof β hairpin. The mobile loop and/or roof β hairpin of several subunits are absent from the X-ray crystal structure of human Hsp10. NMR data suggest that the mobile loop of Hsp10 preferentially samples a hairpin conformation despite the fact that the backbone motion resembles that of a disordered polypeptide. Analysis of backbone dynamics by measurement of ^{15}N relaxation times, T_1 and T_2, and the ^{1}H−^{15}N nuclear Overhauser effect (^{1}H−^{15}N NOE) indicates that motion is greatest near the center of the loop. Inversion of the temperature dependence of the T_1 near the center of the loop marks a transition to motion with a dominant time scale of less than 3 ns. Analysis of the relaxation data by spectral density mapping shows that subnanosecond motion increases uniformly along the loop at elevated temperatures, whereas nanosecond motion increases near the ends of the loop and decreases near the center of the mobile loop. The transition to dominance by fast motion in the center of the loop occurs at a distance from the well-structured part of Hsp10 that is equal to the persistence length of an unstructured polypeptide. Simulation of the spectral density function for the ^{15}N resonance and its temperature dependence using the Lipari−Szabo formalism suggests that the dominant time scales of loop motion range from 0.6 to 18 ns. For comparison, the time scale for molecular rotation of the 70 kDa Hsp10 heptamer is estimated to be 37 ns. Complex behavior of the T_2 relaxation time indicates that motion also occurs on longer time scales. All of the modes of loop motion are likely to have an impact on Hsp10/Hsp60 interaction and therefore affect Hsp10/Hsp60 function as a chaperonin.

The ring-shaped heat shock proteins known as chaperonins promote folding by cycles of ATP-dependent binding and release of nonnative proteins (Zeilstra-Ryalls et al., 1991; Landry & Gierasch, 1994; Hartl, 1996). Almost all of the studies to date on the mechanism of chaperonin function have focused on the *Escherichia coli* GroEL/GroES chaperonin/cochaperonin pair. Similar chaperonin/cochaperonin pairs are found in mitochondria and chloroplasts and are known variously as Hsp60/Hsp10[1] or Cpn60/Cpn10, reflecting their approximate subunit molecular weights of 60×10^3 and 10×10^3, respectively. [An exception is the chloroplast Hsp10 homolog, which has a tandem duplication of the Hsp10 sequence and is called Cpn21 (Baneyx et al., 1995).] Amino acid sequence conservation among Hsp60s and Hsp10s from divergent organisms suggests that the basic elements of their structure and function are conserved (Koonin & van der Vies, 1995; Hunt et al., 1996). Nevertheless, distinct features of mitochondrial biology such as protein import could have imposed distinct requirements on the Hsp60/Hsp10 of that organelle.

Hsp60s and Hsp10s share 7-fold symmetry as befits their subunit-to-subunit interaction in cycles of ATP-dependent binding and dissociation. Electron microscopy of Hsp60s from *E. coli* (Hendrix, 1979; Hohn et al., 1979), yeast mitochondria (McMullin & Hallberg, 1988), and higher plant

† Supported by the National Science Foundation (MCB-9512711), the Louisiana Education Quality Support Fund (1994−97)-RD-A-29, and the Tulane/Xavier Center for Bioenvironmental Research.

‡ Department of Biochemistry.

§ Coordinated Instrumentation Facility.

⊗ Abstract published in *Advance ACS Abstracts,* August 15, 1997.

[1] Abbreviations: CPMG, Carr−Purcell−Meiboom-Gill; HMQC, heteronuclear multiple quantum correlation; HSQC, heteronuclear single quantum correlation; HSMQC, heteronuclear single multiple quantum correlation; NMR, nuclear magnetic resonance; NOE, nuclear Overhauser effect; trNOE, transferred nuclear Overhauser effect; *S*, order parameter; T_1, spin−lattice relaxation time; T_2, spin−spin relaxation time; τ_e, effective correlation time for local conformational fluctuations; τ_m, molecular rotational correlation time; τ_c, generalized correlation time; Hsp60, 60-kDa heat shock protein; Hsp10, 10-kDa heat shock protein; Cpn60, chaperonin 60; Cpn10, chaperonin 10; cDNA, complementary DNA; IPTG, isopropyl 1-thio-β-D-galactopyranoside; DTT, dithiothreitol; DNase I, deoxyribonuclease I; E64, *trans*-epoxysuccinyl-L-leucylamido-(4-guanidino)butane; PMSF, phenylmethanesulfonyl fluoride; EGTA, ethylene glycol bis(β-aminoethyl ether)-*N*,*N*,*N*′,*N*′-tetraacetic acid; EDTA, ethylenediaminetetraacetic acid; DEAE cellulose, diethylaminoethyl cellulose; MES, morpholinoethanesulfonic acid; TMSP, trimethylsilyl propionate; 1D, one-dimensional; 2D, two-dimensional; $^3J_{NH\alpha}$, NH−H$^\alpha$ coupling constant; JR, jump-and-return; R_1, spin−lattice relaxation rate; R_2, spin−spin relaxation rate; δH$^\alpha$, H$^\alpha$ chemical shift; R_{ex}, phenomenological exchange contribution to R_2; $J(\omega_i)$, spectral density function at resonant frequency ω of nucleus type i; f_{rot}, frictional coefficient for rotational diffusion.

S0006-2960(97)01141-0 CCC: $14.00

chloroplasts (Pushkin et al., 1982) reveals a similar organization, 14 subunits arranged in two stacked rings. Surprisingly, a single-ring complex is the predominant form of the recombinant mammalian mitochondrial Hsp60 (Viitanen et al., 1992), but double-ring complexes also are present (P. Viitanen, personal communication). Electron microscopy and other studies show that GroES binds at one end of GroEL with ADP or at both ends with ATP (Langer et al., 1992; Schmidt et al., 1994; Azem et al., 1995; Roseman et al., 1996; Török et al., 1996). Binding of GroES closes the GroEL cavity and simultaneously sequesters its hydrophobic binding sites (Roseman et al., 1996). An unfolded substrate protein can bind in the cavity at either or both ends of the GroEL cylinder, and then GroES can cap the end enclosing the substrate protein (Weissman et al., 1995). GroES binding is thought to trigger release of the substrate into the aqueous interior of GroEL, but escape of the protein into the bulk solvent may require prior dissociation of GroES.

The crystal structures of GroES (Hunt et al., 1996), *Mycobacterium leprae* Hsp10 (Mande et al., 1996), and human Hsp10 (J. F. Hunt, B. J. Scott, L. Henry, J. Guidry, S. J. Landry, and J. Deisenhofer, unpublished results) reveal a molecular frame for dynamic features that mediate intersubunit or intermolecular interactions. Each subunit is composed of a topologically irregular β barrel with two protruding loops. The roof β hairpins extend from the top of the barrels toward the 7-fold axis, giving the molecule a dome-shaped appearance. On the basis of an apparent lack of stabilizing interactions and high crystallographic *B*-factors, the roof β hairpins of GroES were postulated to be metastable (Hunt et al., 1996). If the roof were to become disordered, the 7−10 Å opening at the top of the dome could grow to 25−30 Å, potentially providing an exit route for small folded proteins or unfolded proteins (Hunt et al., 1996). In the crystal structure of the recombinant human Hsp10, six of seven roof β hairpins were not observed, suggesting that they are disordered.

The GroEL-binding mobile loops extend outward from the lower edge of the GroES dome where each may bind to a GroEL subunit at the end of the GroEL cylinder. The 16-residue mobile loops of GroES were first identified by nuclear magnetic resonance spectroscopy (NMR) owing to their unusually high degree of dynamic flexibility (Landry et al., 1993). Subsequently, a 22-residue mobile loop was found in the homologous segment of the GroES homolog encoded by bacteriophage T4, the product of gene *31*, Gp31 (Landry et al., 1996). Interaction of gene *31* with *groEL* and of *groEL* with gene *23*, encoding the T4 capsid protein, suggests that GroEL and Gp31 cooperate in the folding of Gp23 (Zeilstra-Ryalls et al., 1991). Amino acid residues of the GroES and Gp31 mobile loops exhibited well-resolved ^{1}H resonances, and sequence-specific assignments were obtained using two-dimensional homonuclear NMR methods. Only one mobile loop is visible in the crystal structure of GroES, this loop having been immobilized by crystal lattice contacts. Similarly, two mobile loops of human Hsp10 are visible because they are trapped by lattice contacts. The other five mobile loops are disordered. None of the mobile loops are evident in the structure of *M. leprae* Hsp10. Immobilization of the loops when GroES binds to GroEL and localization of *groES*/*groEL* and gene *31*/*groEL* genetic interaction to the loops indicates that the mobile loops mediate an essential interface between GroES and GroEL proteins (Landry et al., 1993, 1996).

The mode of mobile loop binding to GroEL has been analyzed by transferred nuclear Overhauser effects (trNOEs) in nuclear magnetic resonance spectra of synthetic peptides mimicking GroES and Gp31 mobile loops (Landry et al., 1993, 1996). The loop peptides adopt a characteristic hairpin turn and make contact with GroEL through a hydrophobic tripeptide presented on one edge of the hairpin. Since binding to GroEL immobilizes the loop, we proposed that loss of backbone dynamic flexibility acts as an entropic penalty for binding and therefore moderates GroES/GroEL affinity, allowing facile cycling of the complex.

The backbone flexibility of Hsp10 mobile loops is particularly interesting for several reasons: the mobile loops mediate a biologically crucial protein−protein interaction; loop mobility seems to be a key requirement for Hsp10 function; and a target conformation for GroEL-bound mobile loops is known from the peptide trNOE studies. Analysis of NMR relaxation processes provides a means to study backbone dynamics. Flexible segments in a number of native proteins have been studied by NMR. Some flexible segments occur at enzyme active sites, mediate protein−protein interaction, or mediate protein−nucleic acid interaction (Barbato et al., 1992; Redfield et al., 1992; Zink et al., 1994; Nicholson et al., 1995; Cai et al., 1996; Cho et al., 1996; Markus et al., 1997). These segments are less flexible than unfolded polypeptides, and they exhibit significant conformational biases. Other flexible segments are interdomain linkers, which exhibit little evidence of structure (Nowak et al., 1993; Freund et al., 1994; Hansen et al., 1994; Zhou et al., 1996). Nonnative proteins display substantial conformational averaging that is biased toward nativelike structure, depending on how strongly denaturing are the experimental conditions (van Mierlo et al., 1993; Alexandrescu & Shortle, 1994; Logan et al., 1994; Redfield et al., 1994; Farrow et al., 1995a,b, 1997; Zhang & Forman-Kay, 1995, Buck et al., 1996). Generally, backbone motion is at a minimum in the most structured portion of the polypeptides. In a few cases, nonnativelike structural elements were detected in unfolded proteins (Logan et al., 1994; Zhang & Forman-Kay, 1995).

The temperature dependence of NMR relaxation data on proteins and peptides has not been widely examined. In one study on native ribonuclease H, the amplitude of subnanosecond motion was found to increase while its time scale remained constant (Mandel et al., 1996). Another study on both folded and unfolded states of the drkN SH3 domain found that internal dynamics of the folded state changed very little at elevated temperature, whereas the dynamics of the unfolded state increased significantly (Farrow et al., 1997). For the folded protein, the effect of solvent viscosity on molecular tumbling dominated the temperature dependence of the spectral density function at high frequency (516 MHz). In that work, the data were analyzed using both the model-free approach and spectral density mapping.

In the work reported here, NMR methods are used to identify the Hsp60-binding mobile loop in recombinant human Hsp10 and to characterize its backbone dynamics. In addition, we find the roof β hairpin of Hsp10 is flexibly disordered. These flexible segments correspond closely to segments of Hsp10 that were not resolved in the structure

of the Hsp10 heptamer determined by X-ray diffraction with crystals grown in similar solvent conditions. NMR data indicate that the loop preferentially samples a hairpin conformation resembling the conformation that the loop is likely to adopt when bound to Hsp60. The analysis of NMR relaxation processes for the ^{15}N-enriched Hsp10 reveals a complex profile for the mobile loop dynamics. Inversion of the temperature dependence of the spin−lattice relaxation time near the center of the mobile loop provides an independent indication of the dominant time scales of backbone motion. Analysis of the relaxation data and its temperature dependence by spectral density mapping and simulation using the Lipari−Szabo formalism yields an estimate for the range of time scales for mobile loop motion, and it shows that motion broadly shifts to faster time scales at elevated temperature.

EXPERIMENTAL PROCEDURES

Cloning and Expression of Human Hsp10. The cDNA for human Hsp10 was prepared by reverse transcription of total RNA isolated from human umbilical vein epithelial cells followed by amplification using the polymerase chain reaction (PCR) (Gibco/BRL preamplification system and Perkin-Elmer). Primer design was coordinated with the published sequence (Monzini et al., 1994) and incorporated silent mutagenesis for restriction enzyme cleavage and cloning. The amplification product was cleaved with restriction enzymes *Nco*I and *Sac*I and ligated into pET24d (Novagen). The resulting clone, pJG10-2, was verified by DNA sequencing. Expression of Hsp10 was performed in conjunction with the plasmid pLysS (Novagen) encoding the T7 lysozyme in *E. coli* strain BL21(DE3).

Purification of Hsp10. Six 1 L cultures were grown in LB medium with 30 μg/mL kanamycin and 34 μg/mL chloramphenicol at 37 °C. When the cultures reached an A_{600} of 0.8, isopropyl 1-thio-β-D-galactopyranoside (IPTG) (2 mM) was added to induce expression of Hsp10, and incubation was continued for 2 h. Subsequent steps were carried out at 4 °C. Cells were harvested by centrifugation at 1500 rpm and the pellet was resuspended in a final volume of 35 mL with 100 mM Tris-HCl, 5 mM $MgSO_4$, 1 mM dithiothreitol (DTT), and 30 μg/mL DNase I, pH 7.5; protease inhibitors (10 μM E64, 10 μM aprotinin, 1.5 mM PMSF, and 10 mM EGTA) were added; and the cells were lysed by two passes through a French press at 1000 psi. The volume was increased 3-fold, and cell debris was removed by centrifugation at 15 000 rpm. The supernatant was fractionated by ammonium sulfate precipitation; the 0−2.2 M cut was resuspended in 50 mM Tris-HCl and 1 mM EDTA, pH 7.7, and applied to a DEAE-cellulose column equilibrated with the same buffer solution; and the flowthrough containing Hsp10 was separated from many of the remaining proteins by chromatography on an SP Sepharose HP (Pharmacia) column equilibrated with 20 mM MES, pH 6.2, using a linear gradient of 0−1.0 M NaCl. The protein was stored as the precipitate with ammonium sulfate. For preparation of ^{15}N-enriched Hsp10, six 1 L cultures were grown at 37 °C in M9 medium prepared with [^{15}N]ammonium chloride (Cambridge Isotopes) and 0.2% glucose and supplemented with 30 μg/mL kanamycin, 34 μg/mL chloramphenicol, and 0.00005% thiamin hydrochloride. When the cultures reached an A_{600} of 0.6, IPTG was added to induce expression of Hsp10, and incubation was continued for 3 h. Subsequent steps were the same as for preparation of the unlabeled protein.

NMR Data Collection and Processing. Homonuclear NMR experiments were performed on a 3 mM (i.e., ca. 0.43 mM heptamer) sample of unlabeled Hsp10, containing 40 mM potassium phosphate buffer, 8% D_2O (v/v), and traces of NaN_3 and TMSP (pH 6.0, 25 °C). Two-dimensional (2D) NOESY spectra (Jeener et al., 1979; Macura et al., 1981) with mixing times of 100 and 200 ms and HOHAHA spectra (Davis & Bax, 1985) with MLEV-17 or DIPSI-3 (Shaka et al., 1988) of 30−80 ms were recorded with a spectral width of 8000 Hz in both dimensions. Water resonance was suppressed using low-power solvent saturation during the relaxation delay and, in the case of the NOESY experiments, during the mixing time as well or using a "jump-and-return" pulse in place of the last 90° pulse in the NOESY sequence (Plateau & Gueron, 1982), and a 90° "flip-back" pulse followed by a jump-and-return pulse after the DIPSI-3 mixing sequence in the HOHAHA measurements (Bax et al., 1987). Typically, 512 increments of 1024 or 2048 complex data points were collected for each experiment.

Heteronuclear NMR experiments were performed on a 2 mM sample (i.e., ca. 0.29 mM heptamer) of uniformly ^{15}N-enriched Hsp10, containing 40 mM potassium phosphate buffer, 8% D_2O (v/v), and traces of NaN_3 and TMSP. All NMR experiments were recorded on a General Electric Omega PSG 500 MHz spectrometer at 25 °C and pH 6.8, 6.0, 4.2, or 3.5. The pH 3.5 sample was run at five different temperatures, 10, 25, 35, 45, and 55 °C.

2D ^{1}H−^{15}N correlation spectra were collected by heteronuclear single-multiple quantum coherence (HSMQC) (Zuiderweg, 1990), heteronuclear single quantum coherence (HSQC) (Norwood et al., 1990), or heteronuclear multiple quantum coherence with spin−echo water suppression (HMQC-JR) (Sklenar et al., 1987). For sequential assignments, HMQC-NOESY (100, 150, and 300 ms mixing time) and HMQC-HOHAHA (30 and 60 ms mixing time) (Gronenborn et al., 1989; Norwood et al., 1990) with DIPSI-3 mixing scheme (Shaka et al., 1988) experiments were recorded. Typically 128 or 256 increments of 1024 complex data points were collected for each experiment. Spectral widths of 8000 and 1428.57 Hz were used in $F2$ and $F1$, respectively. The ^{1}H carrier was positioned on the H_2O resonance, and the ^{15}N carrier was positioned at 116 ppm. In most experiments water was suppressed using a combination of low-power solvent saturation and trim pulses (Messerle et al., 1989).

Data were processed using Felix 95.0 (MSI). Usually the residual water resonance was removed by convolution before the Fourier transformation (Marion et al., 1989). Zero-filling was employed to yield an absorptive 2D matrix of 1024 × 1024 data points.

To measure $^3J_{NH\alpha}$ coupling constants, a series of HSQC-J data sets were collected, at 35 °C and pH 3.5, with 10 time delays: 10, 30, 50, 60, 70, 80, 90, 100, 110, and 130 ms. For each spectrum a total of 128 real $F1$ and 1024 complex $F2$ points were used with spectral widths of 1428.57 and 8000 Hz, respectively. The 10 sets of data were each treated with identical weighting functions (Lorentz−Gauss in both dimensions) and transformed using the same phase corrections. Zero-filling was employed to yield 2D matrices of 512 × 1024 real data points each. Measured volumes were

plotted as a function of delay time and fit by a curve using nonlinear least-squares methods as described by Billiter et al. (1992).

^{15}N Relaxation Experiments. The pulse sequences used for the measurement of the spin−lattice (T_1) and spin−spin (T_2) relaxation times, together with one of the experiments used to measure heteronuclear Overhauser effects (NOEs) of ^{15}N nuclei in NH groups have been described previously (Kay et al., 1989; Boyd et al., 1990; Palmer et al., 1992). The T_1 relaxation measurements used a series of 9−11 experiments with 8 relaxation delays of 20−2500 ms. T_2 measurements used 12−14 experiments with 9−11 delays of 8.7−348 ms. A recycle delay of 3.0 s was used for the T_1 and 2 s for the T_2 experiments. Typically 64 transients were averaged for each free induction decay. The delay between 180 pulses in the CPMG sequence (2τ) was set to 1 ms. Suppression of the solvent resonance was achieved by low-power presaturation or trim pulses (Messerle et al., 1989). The data sets were acquired on the sample of pH 3.5 at 25, 35, and 45 °C with 128 increments of 1024 complex data points.

Measurement of the ^{1}H−^{15}N NOE requires the acquisition of two experiments, one with ^{1}H decoupling applied during the recycle delay and one without. The NOE was measured using two different pulse sequences. In the first experiment (Kay et al., 1989) water suppression was achieved using short trim pulses (Messerle et al., 1989). For the NOE experiments, where the dynamic range is large, 8 times over sampling in *F*2 was employed. In the experiment with the NOE, the ^{1}H spectrum was saturated by applying a nonselective 135° pulse every 10 ms for a period of 5 s. A series of 1D experiments showed that, after this time, all amide protons were saturated to 99%. The data sets were collected on the sample of pH 3.5 at 25, 35, and 45 °C with 128 increments of 1024 complex data points. Usually 128 transients were acquired for each *t*1 increment. A total recycle delay between transients was set to 5.1 s (greater than 5 times the longest ^{15}N spin−lattice relaxation time). In order to check whether the solvent-saturation transfer limits the quantitative measurement of ^{1}H−^{15}N NOEs using the first pulse sequence with spin−lock purge pulses, the second experiment was carried out in which all proton pulses are replaced with 1-1 (jump-and-return, JR) pulses (Sorensen et al., 1995). Spectra were recorded at 25 and 35 °C, with the JR delay tuned to give intensity maximum at 8.2 ppm. The number of scans per *t*1 increment was 64−128, and the spectral widths were 1428.57 and 10 000 Hz in F1 and F2, respectively.

Calculation of Relaxation Rates and NOEs. The steady-state NOEs were calculated as the ratios of peak heights in the spectrum recorded with proton saturation to those in the spectrum recorded without saturation. Rates R_1 ($=1/T_1$) and R_2 ($=1/T_2$), were fitted as single-exponential decays to peak-height data using a set of scripts written by Dr. Mikael Akke (part of the Dr. Palmer's ModelFree v.3.1 program for optimizing "Lipari−Szabo model-free" parameters to heteronuclear relaxation data).

RESULTS AND DISCUSSION

Assignment of the Mobile Loop and Roof β Hairpin. The uniformly ^{15}N-enriched recombinant human Hsp10 was prepared by overexpression of the cDNA in *E. coli* grown in minimal medium supplemented with [^{15}N]ammonium chloride, followed by purification of the protein using standard chromatographic techniques. The subunit mass, analyzed by high-resolution mass spectrometry (data not shown), is that predicted by the cDNA sequence (Monzini et al., 1994) except lacking the amino-terminal methionine, which also was the case for mouse (Dickson et al., 1994) and rat (Ryan et al., 1995) recombinant Hsp10s. Thus, the recombinant Hsp10 probably differs from the natural protein only by the absence of an amino-terminal acetyl group. Recombinant human Hsp10 is as active as *E. coli* GroES in an assay of GroEL-dependent citrate synthase refolding, and it serves as a cochaperonin with recombinant hamster Hsp60 (A. Garaudy, N. K. Steede, P. Viitanen, and S. J. Landry, unpublished results).

Initial NMR experiments were carried out on the protein dissolved in 40 mM potassium phosphate buffer, pH 6.8, and then the pH was lowered using HCl. Heteronuclear spectra were obtained at pH 6.8, 6.0, 4.2, and 3.5. There was very little difference between spectra obtained at the different pHs aside from some modest changes in NH chemical shifts, suggesting that neither the rigid nor conformationally flexible parts of the protein were significantly affected by changes in pH over the range tested. All subsequent NMR experiments were carried out at pH 3.5 where backbone NH exchange is minimized. It should be noted that the crystals of Hsp10 used to solve the structure by X-ray diffraction were grown at pH 3.5 and in solvent conditions similar to those used for the NMR except with the addition of the precipitant ammonium sulfate (J. F. Hunt, B. J. Scott, L. Henry, J. Guidry, S. J. Landry, and J. Deisenhofer, unpublished results).

Oligomeric forms other than the heptamer are not likely to be substantially populated given the concentration of protein in the NMR sample. Studies on the aggregation behavior of Hsp10 proteins suggests that heptamer formation is highly cooperative. GroES exists in a monomer−heptamer equilibrium characterized by a dissociation constant of approximately 1 μM monomer (Zondlo et al., 1995). Under certain solvent conditions, tetrameric species of the *Mycobacterium tuberculosis* Hsp10 and human Hsp10 have been observed (Fossati et al., 1995). However, the tetrameric species were noted only for samples with monomer concentrations below 100 μM. Where higher concentrations were tested, the dominant species was the heptamer.

Backbone and many side-chain ^{15}N and ^{1}H resonances from flexibly disordered segments of the recombinant human Hsp10 were assigned using a combination of ^{1}H,^{15}N heteronuclear spectra (HSQC, HMQC-NOESY, and HMQC-HOHAHA). Two continuous segments were identified, A21−G38 and K55−E58 (Figures 1 & 2).

Strikingly, the mobile loop segment (A21−G38) of Hsp10 corresponds almost exactly to the mobile loop segment previously identified in GroES. Precisely the same amino acid residues are not observed for several subunits in the crystal structure of Hsp10 (J. F. Hunt, B. J. Scott, L. Henry, J. Guidry, S. J. Landry, and J. Deisenhofer, unpublished results), suggesting that there is a sharp transition between ordered and disordered polypeptide chain. In view of the disposition of the mobile loops in the GroES and Hsp10 crystal structures, loop flexibility evidently begins at the point where the polypeptide chain exits the β barrel domain and ends at the point of reentry (Figure 3). In the crystal structure

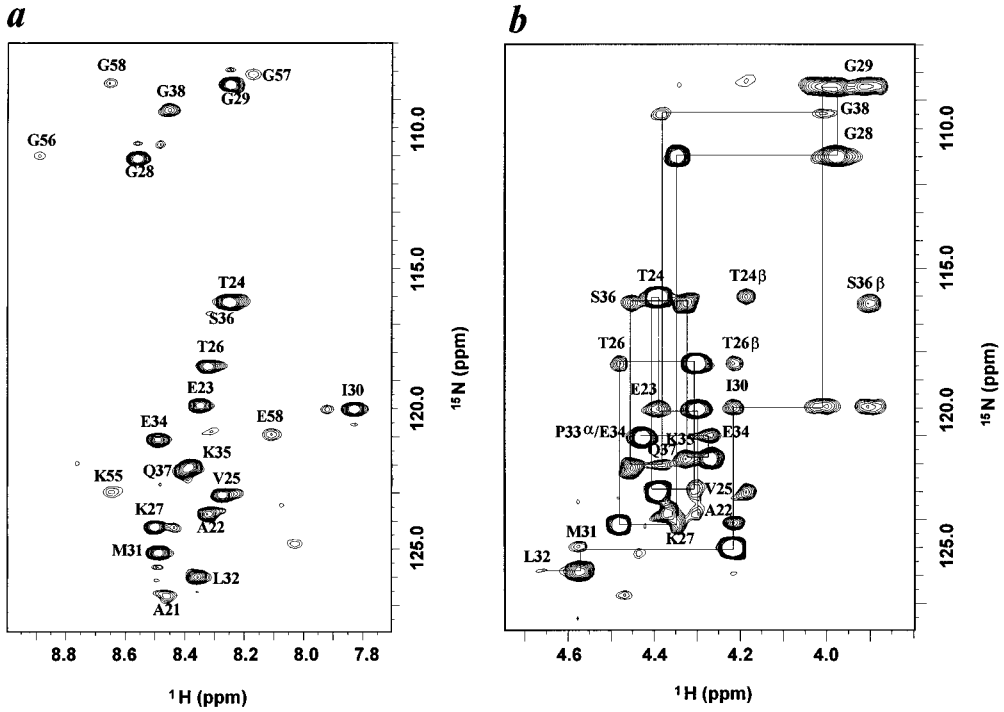

FIGURE 1: Assignment of mobile segments in human Hsp10. $^1H-^{15}N$ amide correlations for residues of both the mobile loop (A21−G38) and roof β hairpin (K55−E58) are labeled in the HSQC spectrum (a). Note the weak intensity of cross peaks for A21, G38, and residues of the roof β hairpin due to line broadening. The sequential assignment of the mobile loop is indicated in the H^α region of the HMQC-NOESY spectrum (b). Only the intraresidue correlations are labeled. A break in the sequential assignment occurs at P33 for lack of an amide proton.

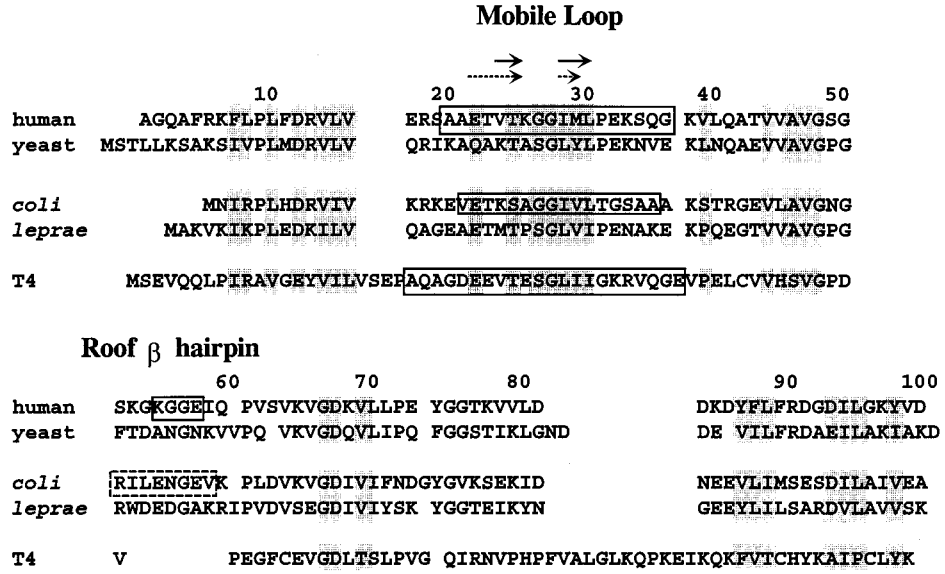

FIGURE 2: Alignment of Hsp10 sequences [adapted from Hunt et al., 1997)]. Mobile loops and roof β hairpins characterized by NMR are indicated with solid boxes. The roof β hairpin of GroES is indicated with a broken box (Hunt *et al.*, 1996). Solid arrows indicate positions predicted to form antiparallel strands in the Hsp60-bound hairpin conformation of the mobile loop (Landry *et al.*, 1996). Broken arrows indicate positions that tend to form an extended conformation in the free Hsp10 protein. Conserved sequence positions are highlighted in gray (Koonin & van der Vies, 1995).

of Hsp10, the NH of S20 is hydrogen bonded to the CO of Q42, and therefore the first and last residues of the mobile loop lie close to each other. Clearly the chain reverses direction in the course of the mobile loop.

In addition to the mobile loop, four residues (K55−E58) of the roof β hairpin are sufficiently dynamic to be assigned. This observation is not surprising since the entire roof β hairpin (S52−Q60) of some Hsp10 subunits is not seen in the crystal structure. The assigned residues are only just mobile enough to be observed by NMR. Cross peaks involving K55 and E58 could be identified only in spectra obtained at 35 °C and above. Presumably, residues observed neither by crystallography nor by NMR are disordered, but their motion is too slow to give sufficiently narrow resonance lines at this magnetic field strength. While not as flexible as in Hsp10, the roof β hairpin of GroES has high crystallographic *B*-factors and was predicted to be metastable due to a paucity of stabilizing interactions. Flexibility in roof β hairpins favors the possibility that a protein substrate may exit from the Hsp60/Hsp10 complex through the roof

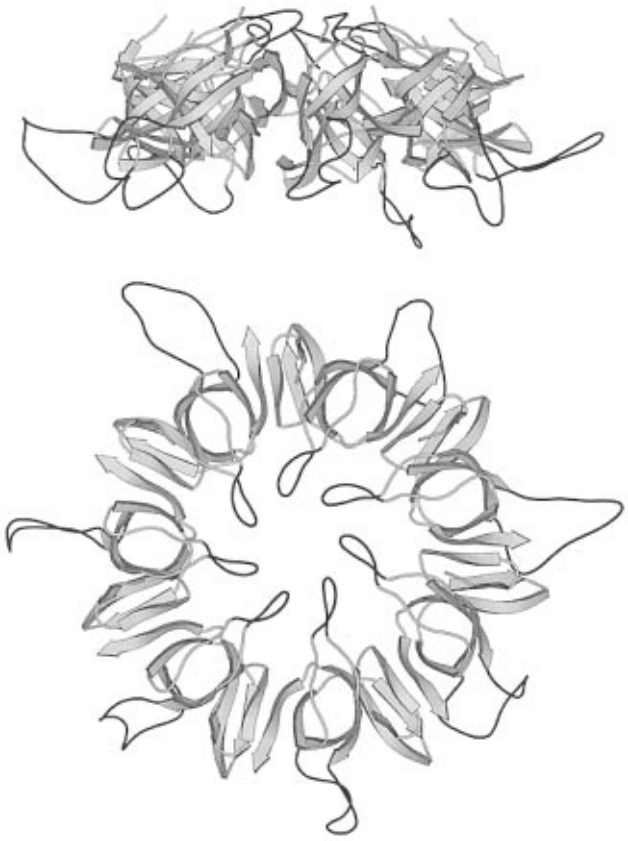

FIGURE 3: Ribbon diagrams of human Hsp10 showing the location of the mobile loops and roof β hairpins. The "side" view of the dome-shaped heptamer is shown in the upper panel, and the "top" view is in the lower panel. Structural data on the well-ordered portion of the molecule were provided by J. F. Hunt, B. J. Scott, L. Henry, J. Guidry, S. J. Landry, and J. Deisenhofer, (unpublished results). Flexible segments that are absent from the crystal structure and include residues identified by NMR are indicated in solid black. Hsp60-binding mobile loops extend outward from the lower edge of the dome. Roof β hairpins point inward to the 7-fold axis. The hypothetical conformations of the mobile loops were generated by molecular dynamics and simulated annealing, and the conformation of the roof β hairpins was generated by homology modeling using GroES as a template. The diagrams were prepared using the program MOLSCRIPT (Kraulis, 1991).

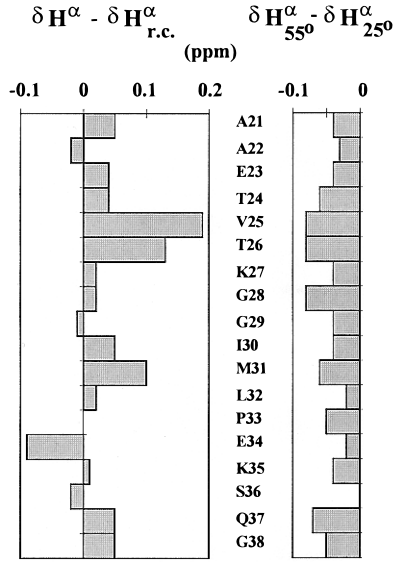

FIGURE 4: H^α chemical shift deviation from random coil values and change with temperature. Values of δH^α at 25 °C for mobile loop residues (except L32) were subtracted from random coil values reported by Wishart et al. (1992). The value for L32 was subtracted from the value observed for L followed by P in a model peptide (Wishart et al., 1995). δH^α values for V25, T26, and M31 exhibit deviations greater than 0.1 ppm upfield. Upfield deviation is associated with β sheet secondary structure. A tendency for these residues to be in a β (or extended) conformation is consistent with formation of a nascent hairpin that resembles the GroEL-bound conformation determined by trNOE NMR for the GroES mobile loop peptide (Landry et al., 1996). At increased temperature, the δH^α of several residues including the aforementioned moves downfield, suggesting a change in the conformational bias of the loop.

of the Hsp10 (Hunt et al., 1996). The T4 Hsp10 Gp31 was predicted to lack a roof β hairpin altogether (Landry et al., 1996), and this was borne out by the recent solution of its crystal structure (Hunt et al., 1997).

A Nascent Hairpin in the Mobile Loop. Despite the highly dynamic behavior of the mobile loop, NMR data indicate that the mobile loop samples a preferred conformation containing a turn near the center of the loop. As expected from the loop's flexible mobility, most of the H^α chemical shifts (δH^α) are within 0.1 ppm of random coil values (Figure 4). However, δH^α of three residues (V25, T26, and M31) have values shifted greater than 0.1 ppm downfield, which suggests they tend to adopt an extended or β conformation (Wishart et al., 1992). Information on the backbone conformation can be obtained from NH−H^α coupling constants ($^3J_{NH\alpha}$); thus, the HSQC-J experiment was performed, and $^3J_{NH\alpha}$ were determined for all loop residues except Q37 (low intensity), G28, G29, and G38 (ambiguity of two H^α) and P33 (no NH). Values of $^3J_{NH\alpha}$ in hertz are as follows: A21, 6.7; A22, 5.5; E23, 7.1; T24, 7.7; V25, 7.7; T26, 7.7; K27, 6.2; I30, 7.7; M31, 7.1; L32, 6.2; E34, 5.9; K35, 6.3; and S36, 6.7. Unbiased conformational averaging of the backbone dihedral angle ϕ yields $^3J_{NH\alpha}$ in the range 6−7 Hz (Dyson & Wright, 1991). Values below this range indicate a bias toward helical conformation, and values above this range indicate a bias toward extended or β conformation. A number of the $^3J_{NH\alpha}$ for loop residues are in excess of 7 Hz (E23−T26, I30, M31); thus they tend to adopt an extended conformation. Nevertheless, these residues spend only a fraction of the time in an extended conformation as $^3J_{NH\alpha}$ for residues in β structure of native proteins typically are 8−10 Hz. The combination of elevated δH^α and elevated $^3J_{NH\alpha}$ at identical or adjacent residues indicates a bias toward an extended conformation in the segments E23−T26 and I30−M31.

As expected for a largely disordered polypeptide, no medium- or long-range $^1H-^1H$ NOEs are observed. However, most sequential NH/NH NOEs are evident, including a strong one corresponding to G29/I30 (Figure 5). Any type of tight turn should produce at least one strong sequential NH/NH NOE, and G29/I30 lies between two segments that are biased toward the extended conformation (Figure 2). Since the chain must reverse itself between the loop ends, a favored conformation is likely to be a β hairpin centered on residues K27-G28-G29. This predicted site for a turn is homologous to the sequence (A22-G23-G24) that forms a turn in the GroES mobile loop peptide while bound to GroEL (Landry et al., 1996). It is reasonable that the conformation adopted by the loop upon binding to GroEL should be one of its more favored conformations in the free protein. A similar conformational bias was evident in spectra of GroES and Gp31, in which the NH/NH NOEs homologous to that of Hsp10 G29/I30 also were prominent (Landry et al., 1996).

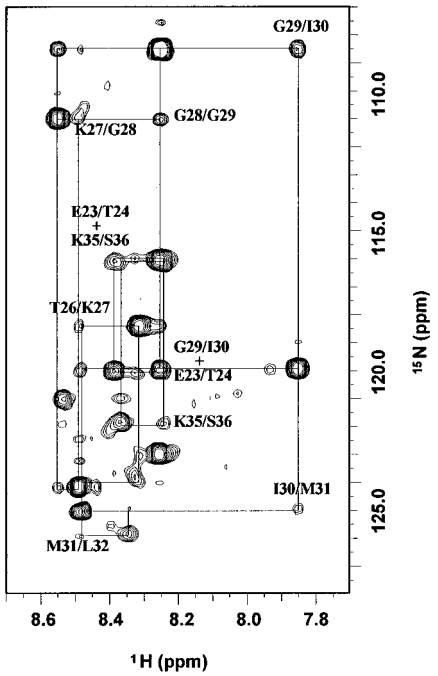

FIGURE 5: Sequential NH−NH NOEs in the mobile loop. Cross peaks between sequential NH resonances are labeled in this portion of the HMQC-NOESY spectrum of Hsp10 (NOESY mixing time, 150 ms). The largest cross peak corresponds to an NH−NH NOE between G29 and I30, suggesting a tendency to form a turn. In previous work, strong NH−NH NOEs were observed between residues homologous to G29 and I30 in GroES and Gp31, and these residues are located in the turn described by trNOE NMR for the GroEL-bound conformation of the GroES and Gp31 mobile loop peptides (Landry et al., 1996).

Features of mobile loop dynamic flexibility are evident in the T_1 and T_2 relaxation times of the backbone amide [^{15}N]nitrogens and in the intensity and sign of the ^{1}H−^{15}N NOEs (Figure 6). ^{1}H-detected ^{15}N relaxation and NOE experiments were performed at 25, 35, and 45 °C. The T_1 and T_2 data shown are from single experiments. The NOE data shown are from the average of two experiments each at 25 and 35 °C and from a single experiment at 45 °C. Precision was evaluated for replicates of the experiments as well as in the fitting of a single data set. Errors associated with means for three T_1 and T_2 experiments were slightly greater than errors associated with fitting individual data sets; thus, only the errors associated with the means for three experiments are discussed. Generally, the errors are larger at the loop ends due to the low intensity of the cross peaks. The error in the mean for three T_1 experiments at 25 °C was in the range 1.5−3.9% for residues A22−Q37 and was 7.4% and 11.0% for residues A21 and G38, respectively. The error in the mean for three T_2 experiments was in the range 0.5−1.5% for residues A22−Q37 and was 6.2% and 4.3% for residues A21 and G38, respectively. Reproducibility in the NOE results was assessed by a single replicate each at 25 and 35 °C. Generally, the errors are larger near the ends of the loop, where the NOE approaches zero and the intensity of the peaks also is low. Standard error of the mean between the two experiments was in the range 1.1−12% for residues E23−L32 and 3−32% for residues E34−G38. The value of the NOE for A21 and A22 deviated by severalfold between the two experiments.

At all temperatures, most of the NOEs are negative, which is characteristic of disordered polypeptide segments. Generally, all three measures, T_1, T_2, and NOE, indicate greater mobility toward the center of the loop. This feature suggests that the most significant attachment of the loop to the rigid portion of Hsp10 is through the covalent bonds of the polypeptide backbone at the loop ends.

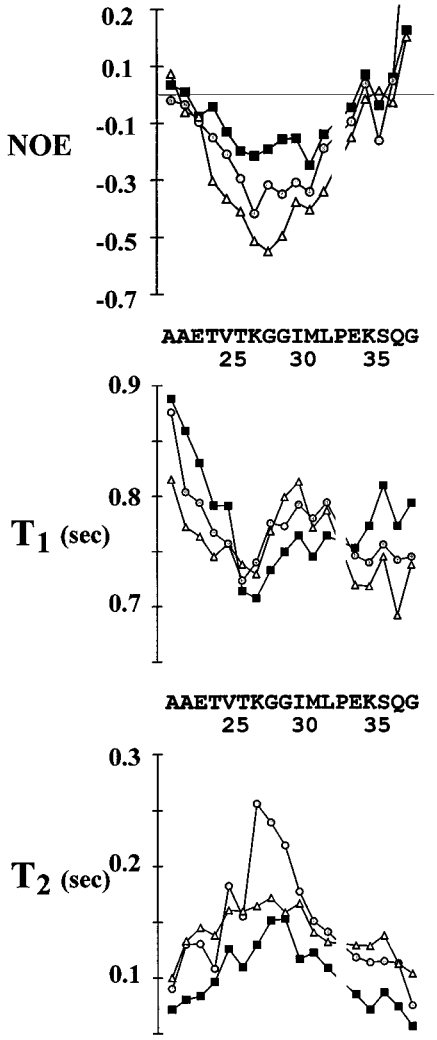

FIGURE 6: ^{1}H−^{15}N nuclear Overhauser effects of mobile loop amide groups and spin−lattice (T_1) and spin−spin (T_2) relaxation times for mobile loop amide [^{15}N]nitrogens at 25 °C (black squares), 35 °C (gray circles), and 45 °C (open triangles). At most residue positions, the NOE is negative, which is typical for highly disordered polypeptide chains. Two maxima at K27 and M31 at 25 °C could result from a conformational bias. The altered profile at higher temperatures indicates a change in the distribution of motion and therefore suggests a change in conformational bias. The temperature dependence of the T_1 is inverted for residues in the middle of the loop (T26−L32), indicating motion dominated by a time scale shorter than 3 ns for that segment. The T_2 goes through a maximum near the center of the loop, and the T_2 for all mobile loop residues increases as the temperature rises from 25 to 35 °C, as expected for increased fast motion. However, T_2 decreases upon further heating to 45 °C. Thus, a microsecond to millisecond exchange process makes a more significant contribution to spin−spin relaxation in this temperature range.

Inversion of the T_1 temperature dependence in the middle of the mobile loop provides a reference point for the time scale of loop motion. In a simple model for the relaxation of an amide nitrogen atom experiencing isotropic motion, T_1 as a function of correlation time (τ_c) goes through a minimum near 3 ns in a 500 MHz field; thus the temperature dependence of T_1 is inverted upon passing through this minimum. T_1 decreases with increasing temperature for

amide groups having $\tau_c > 3$ ns; whereas T_1 increases with increasing temperature for amide groups having $\tau_c < 3$ ns. The temperature dependence of T_1 for most mobile loop amides is consistent with motion having $\tau_c > 3$ ns. However, a few amides in the center of the loop (T26−L32) exhibit longer T_1 at elevated temperature and therefore experience motion having $\tau_c < 3$ ns.

Different dynamics measures indicate slightly different positions of maximum mobility in the loop, and the maxima change with temperature. The various relaxation mechanisms are sensitive to motion on different time scales. Thus, a complex harmony of conformational fluctuations may yield a complex relaxation profile. At 25 °C, maxima in the NOE profile occur at K27 and M31, but they are progressively overtaken by a single maximum at G28 as the temperature is raised to 35 and 45 °C. Maximum flexibility indicated by T_1 occurs near I30. Although the maximum in T_2 occurs near the middle of the loop, interpretation of T_2 in terms of loop motion is severely compromised by a contribution from chemical exchange (see below).

Changes in δH^α with increasing temperature over the range 25−55 °C suggest a change in conformational behavior (Figure 4). The δH^α for six residues (T24, V25, T26, G28, M31, and Q37) move upfield 0.06 ppm or more. Since the δH^α of T24, V25, T26, and M31 deviate downfield at 25 °C, the upfield movement at elevated temperature suggests that the conformational behavior of these residues becomes less biased toward extended conformation and more like a random coil. In contrast, the upfield movement of the G28 δH^α results in an upfield deviation from random coil values at 55 °C, suggesting a tendency toward turn formation. All of the residues exhibiting strongly temperature-dependent δH^α except Q37 are implicated in formation of a hairpin turn upon binding to Hsp60 by homology to residues in the GroES mobile loop. In particular, V25 and M31 correspond to residues (K20 and V26) in GroES that lie next to each other on opposite strands of the hairpin. We suspect that juxtaposition of these residues in the nascent hairpin structure contributes to concerted changes in δH^α.

Spectral Density Mapping of Backbone Motion. Two general frameworks for analyzing backbone dynamics have been applied to NMR relaxation data, the model-free approach (Lipari & Szabo, 1982a,b; Kay et al., 1989; Clore et al., 1990a,b) and spectral density mapping (Peng & Wagner, 1992; Farrow et al., 1995b; Ishima & Nagayama, 1995). The model-free approach breaks down backbone motion into various time scales and weights their contributions. Various forms of spectral density function are constructed with two or three correlation times (including one for the molecular rotation) and one or two order parameters. Usually, the molecular rotational correlation time (τ_m) is estimated from values of T_1/T_2 for residues in the most well-organized parts of the protein. A best fit of all relaxation measures for each residue is obtained with the various forms of spectral density function. Initially the simplest form is attempted and then progressively more complicated forms are tried. Some residues require a phenomenological chemical exchange term (R_{ex}) in the equation for T_2 in order to obtain an adequate fit (Palmer et al., 1991).

Several properties of Hsp10 render unsuitable the strategy to globally fit the relaxation data with the model-free formalism. First, any single estimate of τ_m seems unreliable or inappropriate. Our estimates of τ_m range from 37 ns using HYDRO (de la Torre et al., 1994) with the X-ray crystal structure to less than 18 ns by graphical simulation of the relaxation data and its temperature dependence (see below). Second, the molecular rotation of Hsp10 is expected to be strongly anisotropic, and thus the value of τ_m will depend on the relative orientation of the particular NH bond vector with the axes of molecular rotation. The dome-shaped Hsp10 heptamer may be described as an oblate ellipsoid with an axial ratio of 2.5, and the mobile loops extending from the lower edge must also affect the molecular rotation. Third, the magnitude of the phenomenological chemical exchange term is large, and therefore associated errors are likely to severely distort the analysis. T_2 measurements carried out at three different CPMG periods (1, 0.5, and 0.25 ms) suggest that chemical exchange makes a significant contribution, but the data were not readily interpretable. Furthermore, the dramatic decrease in T_2 upon increasing the temperature from 35 to 45 °C may derive only from a large increase in R_{ex}.

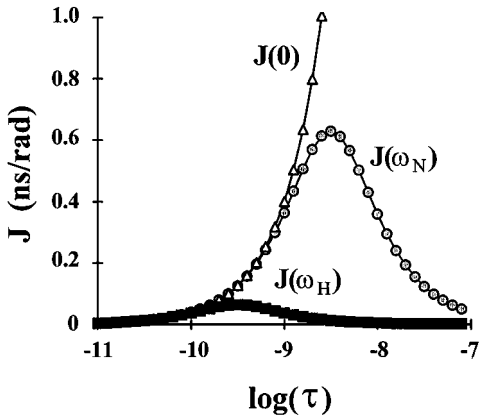

FIGURE 7: Spectral density functions as a function of correlation time for an amide experiencing isotropic motion. The maximum in $J(\omega_H)$ occurs at approximately 0.3 ns, and in $J(\omega_N)$, at 3 ns. Data points were elaborated with the equation $J(\omega) = (^2/_5)\tau/[1 + (\omega\tau)^2]$, where $\omega_H = 500$ MHz and $\omega_N = 50$ MHz.

Spectral density mapping is a more straightforward method to analyze backbone dynamics. Spectral density mapping can evaluate the breadth of backbone motions as well as assess the extent of motion on the time scales of the experimentally measured resonances. Theoretical curves are presented for the three spectral density functions as a function of correlation time for an isotropic rotor (Figure 7). Since $J(0)$ is affected by chemical exchange, it is underestimated in the present case and will not be discussed. However, $J(\omega_H)$ and $J(\omega_N)$ are determined only from the values of T_1 and NOE and therefore are insensitive to any contribution to T_2 from chemical exchange. From these plots, it can be appreciated that the response of the spectral density function to faster motion (for example, at elevated temperature) depends on the effectiveness with which the spectral density function samples the dominant time scale of motion. For measurements at a magnetic field of 11.7 T ($\omega_H = 500$ MHz), $J(\omega_H)$ most effectively samples motion near a time scale of 0.3 ns, whereas $J(\omega_N)$ samples most effectively near a time scale of 3 ns. At elevated temperature, motions redistribute to faster time scales and the spectral density function may increase or decrease. For example, when the dominant time scale is slower than 3 ns, $J(\omega_N)$ increases; when it is faster than 3 ns, $J(\omega_N)$ decreases.

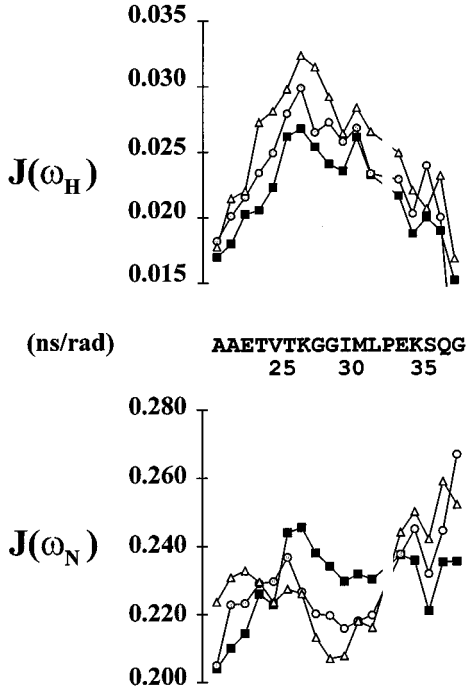

FIGURE 8: Spectral density functions for mobile loop amide groups at 25 °C (black squares), 35 °C (gray circles), and 45 °C (open triangles). The magnitude and temperature dependence describe the extent that backbone motion samples motion on the corresponding time scales. As expected for motion near the nanosecond time scale, the profiles of $J(\omega_H)$ and $J(\omega_N)$ resemble the profiles of T_1 and the NOE, respectively. $J(\omega_H)$ increases almost uniformly over the length of the mobile loop, suggesting that there is a uniform acceleration of local conformational fluctuation. As in the profile of T_1, the inverted temperature dependence of $J(\omega_N)$ indicates a transition to predominantly fast motion in the center of the loop. The length of chain from the fixed ends of the loop to the transition to fast motion is approximately five residues, equal to the persistence length of an unstructured polypeptide (Cantor & Schimmel, 1980).

The T_1 and NOE were fitted to simplified equations based on the spectral density functions, $J(\omega_H)$ and $J(\omega_N)$ (Farrow et al., 1995b). Plots of $J(\omega_H)$ and $J(\omega_N)$ calculated from the relaxation data reveal how motion on these two time scales is distributed in the mobile loop (Figure 8). $J(\omega_H)$ exhibits a profile similar to (1 − NOE), and $J(\omega_N)$ exhibits a profile similar to $1/T_1$. These similarities are rationalized as follows. The equation for $1/T_1$ is a linear combination of terms in $J(\omega_N)$ and $J(\omega_H)$ with comparably sized coefficients. Since $J(\omega_N)$ is much larger than $J(\omega_H)$ for amides experiencing motion predominantly on the nanosecond time scale, the equation is dominated by $J(\omega_N)$. The equation for the NOE is essentially one plus the product of $5J(\omega_H)$ and T_1. In the present data as well as other studies, T_1 varies by no more than approximately 50%. Thus, a comparable amount of variation in $J(\omega_H)$ dominates the NOE by a factor of 5.

The backbone dynamics and especially their temperature dependence are conveniently interpreted in terms of $J(\omega_H)$ and $J(\omega_N)$. $J(\omega_H)$ rises with temperature almost uniformly over the length of the mobile loop, indicating more rapid local chain dynamics. Near the ends of the loop, $J(\omega_N)$ increases with elevated temperature. Presumably, this reflects more rapid molecular rotation and/or large-scale conformational fluctuations. In the middle of the loop, $J(\omega_N)$ decreases with elevated temperature, as expected for a redistribution of motion to faster time scales. The transition to dominance by fast motion occurs five residues from both

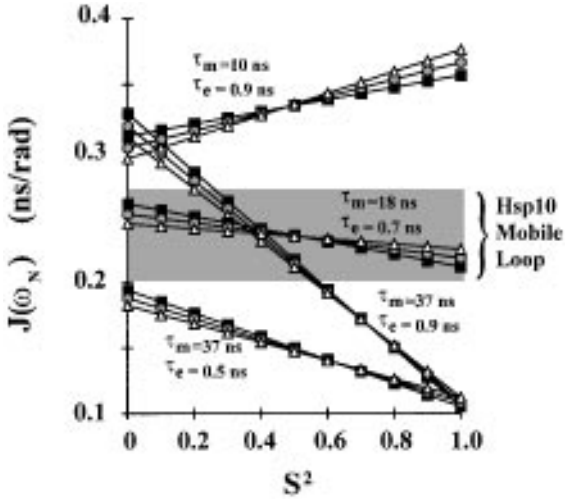

FIGURE 9: Simulations of the spectral density function $J(\omega_N)$ at 25 °C (black squares), 35 °C (gray circles), and 45 °C (open triangles). Data points were elaborated with the equation $J(\omega) = (^2/_5)\{S^2\tau_m/[1 + (\omega\tau_m)^2] + (1 - S^2)\tau/[1 + (\omega\tau)^2]\}$, where $\tau = \tau_m\tau_e/(\tau_m + \tau_e)$. The indicated values of τ_m and τ_e correspond to the simulation at 25 °C. The values of τ_m and τ_e at 35 and 45 °C were obtained by the relation $\tau_T = 298\tau_{298}/T$, where T is the temperature in kelvins.

the N- and C-terminal ends. Since the persistence length of a disordered polypeptide is approximately five residues (Cantor & Schimmel, 1980), these transitions may simply reflect the diminished influence of molecular rotation on local relaxation rates. The propagation of nanosecond (or slower) motion along the chain is washed out by fast local dynamics.

Graphical simulation of $J(\omega_N)$ and its temperature dependence using the Lipari−Szabo model-free formalism permits the estimation of an operationally defined τ_m and an effective correlation time for local conformational fluctuation (τ_e) (Figure 9). In this simulation, τ_m is not likely to correspond to the molecular rotation. Hsp10 may not be sufficiently rigid for the molecular rotation to be captured in the properties of any of its individual atoms, let alone those of the mobile loop. Nevertheless, an operationally defined τ_m serves as a useful benchmark to differentiate where in the polypeptide slow and fast motions dominate. The temperature dependence of τ_m and τ_e is assumed to be controlled by "stick" boundary conditions for rotational diffusion and therefore varies as a function of $f_{rot}/2kT$, where f_{rot} is the frictional coefficient for rotational diffusion, k is the Boltzmann constant, and T is the temperature in kelvins. This assumption contrasts with the temperature-independent behavior of τ_e observed for folded ribonuclease H (Mandel et al., 1996). However, in the RNase H system, τ_e is believed to reflect the time scale of jumps between nearly isoenergetic conformational states. In the case of the mobile loop, τ_e is more likely to be dominated by segmental motion that is resisted by solvent viscosity. The simulations generate values of $J(\omega_N)$ in the experimentally observed range when the correlation times are as follows: 14 ns $< \tau_m <$ 18 ns and 0.6 $< \tau_e <$ 0.7 ns. Within this regime of time scales, inversion of the temperature dependence occurs near $S^2 = 0.5$. It is reasonable that this value should coincide with a distance from the loop ends that is equivalent to the persistence length of an unstructured polypeptide.

The magnitude of the simulated $J(\omega_N)$ temperature dependence for $S^2 = 0$ (3.3% per 10 °C) is less than half the magnitude observed for residues in the middle of the loop

(7.2% for K27 between 25 and 35 °C). Perhaps this disparity points to conformational fluctuations that are not adequately simulated as rotation. Motion with a translational component (*e.g.*, "swinging" of the loop) is expected to have a much higher frictional coefficient and therefore larger temperature dependence.

CONCLUSIONS

The roof β hairpin of human Hsp10 is sufficiently disordered that it is observed by solution-phase NMR. This result strongly suggests that the absence of roof β hairpins from the crystal structure of Hsp10 is explained by their dynamic flexibility in the crystal. The existence of the roof β hairpins remains something of an enigma, but these results support the earlier suggestion that under some circumstances the roof β hairpins open a channel to the folding chamber in the chaperonin complex (Hunt et al., 1996). Whether protein substrates or other molecules normally pass through this aperture remains unknown.

The high degree of dynamic flexibility in the human Hsp10 mobile loop confirms that disorder is a conserved feature of this Hsp60-binding loop in Hsp10s of eukaryotic mitochondria as well as of bacteria. Thus, flexibility itself is a functionally important characteristic. We have proposed that flexibility allows the Hsp10/Hsp60 complex to accommodate substrate-specific distortions when the Hsp10 binds to an Hsp60-substrate complex. The near-identical length of mobile loops in human Hsp10 and *E. coli* GroES may reflect optimization of these Hsp10s for a similar spectrum of substrate proteins. On the other hand, the longer mobile loop of the T4 Hsp10 Gp31 may facilitate Gp31/GroEL-assisted folding of a single substrate, the T4 capsid protein Gp23. Perhaps the longer loops allow Gp31 to "reach around" GroEL-bound Gp23. At 56 kDa, Gp23 is among the largest proteins thought to depend on an Hsp10 for folding.

We have proposed that mobile loop disorder moderates the affinity of Hsp10 binding to Hsp60. The conformational behavior of the loop seems to be biased to adopt the Hsp60-bound conformation, but it must not be preordered to the extent that binding is too tight. The multivalent interaction between Hsp10 and Hsp60 amplifies sensitivity to binding affinity. Thus, binding and dissociation are delicately balanced by the interplay of mobile loop structure and dynamics.

The pyrrolidine ring of P33 could restrain backbone mobility in the carboxy-terminal portion of the mobile loop. Mutation of P33 to any other residue should substantially increase mobility and therefore reduce Hsp60 binding affinity. Two research groups independently isolated temperature-sensitive mutants in the gene for yeast Hsp10 that specified substitutions for proline in the position homologous to P33 (Hohfeld & Hartl, 1994; Dubaquié et al., 1997). In the study by Hohfeld and Hartl (1994), the temperature-sensitive defect was recapitulated *in vitro*. Hsp10 binding to GroEL was lost at the nonpermissive temperature and recovered upon shift to the permissive temperature. These authors concluded that the defective protein could revert to the active form. This behavior may be explained by excessive disorder in the mutant mobile loop. If the dynamic flexibility is too great, then the entropy loss upon binding may be too unfavorable.

Temperature-dependent changes in Hsp10 structure and dynamics provides a mechanism for regulation of Hsp60 activity. The increase in mobile loop dynamics at elevated temperature must increase the entropic cost of ordering the loop upon Hsp60 binding. Reduced Hsp10/Hsp60 affinity might result unless the greater entropic cost is compensated by other changes in the interaction that favor binding, such as enhanced hydrophobic interaction, altered behavior of Hsp60, or possibly changes in the conformational bias of the mobile loop. Indeed, a reduction in GroES/GroEL complex formation was observed at elevated temperature (Goloubinoff et al., 1997). However, since ATP hydrolysis is accelerated at elevated temperature, it remains unclear whether this is due to reduced GroES−GroEL affinity or a reduced steady-state level of GroEL(ATP).

The deviations in δH^{α} and $^{3}J_{NH\alpha}$ from random coil values and the complex profile of loop dynamics suggest that the conformational behavior of the loop is biased toward a hairpin conformation, and the conformational bias is reduced at elevated temperature. It will be interesting to examine how mutations affect the conformational behavior of the loop. We suspect that some mutations will increase Hsp60 binding affinity by further preordering of the loop in the Hsp60-binding conformation.

The temperature dependence of the T_1 and NOE provides a useful measure of the time scale of backbone dynamics that is not compromised by microsecond to millisecond exchange processes. In the case of the mobile loop, the temperature dependence of T_1 and $J(\omega_N)$ are inverted for residues near the middle of the loop. Thus, these residues experience motion dominated by a time scale shorter than 3 ns, and this motion is subject to frictional drag. Simulation of $J(\omega_N)$ in terms of the model-free formalism using an operationally defined molecular correlation time (τ_m), an effective correlation time for local conformational fluctuations (τ_e), and an order parameter (S^2) shows that the influence of well-ordered parts of the molecule on local dynamics fades as predicted by the persistence length of an unstructured polypeptide. The simulation suggests that the longest time scale of motion experienced by the NMR-accessible loop residues is approximately 18 ns. This is considerably shorter than the time scale predicted for molecular rotation of the Hsp10 heptamer on the basis of the X-ray crystal structure. The discrepancy could be due to large-scale conformational fluctuations in the loop or vibrational modes in the Hsp10 ring. Notably, a microsecond to millisecond exchange process is present at 25 °C, and it becomes much more pronounced at 45 °C. The nature of this process is unknown. One potential cause is the dissociation of the heptamer into monomers. Although GroES undergoes dissociation on the time scale of minutes at 25 °C (Zondlo et al., 1995), dissociation of human Hsp10 in our experimental conditions might be sufficiently fast to cause exchange broadening. The fastest motion in the loop, characterized by $\tau_e \sim 0.6$ ns, is comparable to the time scale of segmental motion previously reported for nonnative proteins (Allerhand et al., 1971; Torchia et al., 1975; Alexandrescu & Shortle, 1994).

The studies reported here provide a fairly detailed picture of the mobile loop's dynamic conformational behavior. The wide range of time scales of motion observed in this short length of peptide and the variety of structural information

already available makes this system attractive for molecular dynamics simulation.

ACKNOWLEDGMENT

We thank J. Hunt, B. J. Scott, L. Henry, J. Guidry, and J. Deisenhofer for providing the crystal structure of human Hsp10 prior to publication; Jesse Guidry for the kind gift of the Hsp10 overexpresser strain; J. Boyd for pulse sequences; N. Farrow for the program for spectral density mapping; and A. Alexandrescu, J. Boyd, T. Holak, and D. Torchia for critically reading the manuscript.

SUPPORTING INFORMATION AVAILABLE

Three tables containing T_1, T_2, NOE, $J(\omega_H)$, and $J(\omega_N)$ values for the human Hsp10 mobile loop at 25, 35, and 45 °C (2 pages). Ordering information is given on any current masthead page.

REFERENCES

Alexandrescu, A. T., & Shortle, D. (1994) *J. Mol. Biol. 242*, 527−546.
Allerhand, A., Doddrell, D., Glushko, V., Cochran, D. W., Wenkert, E., Lawson, P. J., & Gurd, F. R. N. (1971) *J. Am. Chem. Soc. 93*, 544−546.
Azem, A., Diamant, S., Kessel, M., Weiss, C., & Goloubinoff, P. (1995) *Proc. Natl. Acad. Sci. U.S.A. 92*, 12021−12025.
Baneyx, F., Bertsch, U., Kalbach, C. E., Vandervies, S. M., Soll, J., & Gatenby, A. A. (1995) *J. Biol. Chem. 270*, 10695−10702.
Barbato, G., Ikura, M., Kay, L. E., Pastor, R. W., & Bax, A. (1992) *Biochemistry 31*, 5269−5278.
Bax, A., Sklenar, V., Clore, G. M., & Gronenborn, A. M. (1987) *J. Am. Chem. Soc. 109*, 6511−6513.
Billiter, M., Neri, D., Otting, G., Qian, Y. Q., & Wüthrich, K. (1992) *J. Biomol. NMR 2*, 257−274.
Boyd, J., Hommel, U., & Campbell, I. D. (1990) *Chem. Phys. Lett. 175*, 477−482.
Buck, M., Schwalbe, H., & Dobson, C. M. (1996) *J. Mol. Biol. 257*, 669−683.
Cai, M. L., Huang, Y., Prakash, O., Wen, L., Dunkelbarger, S. P., Huang, J. K., Liu, J. H., & Krishnamoorthi, R. (1996) *Biochemistry 35*, 4784−4794.
Cantor, C. R., & Schimmel, P. R. (1980) *Biophysical Chemistry*, W. H. Freeman, New York.
Cho, H. S., Liu, C. W., Damberger, F. F., Pelton, J. G., Nelson, H. C. M., & Wemmer, D. E. (1996) *Protein Sci. 5*, 262−269.
Clore, G. M., Driscoll, P. C., Wingfield, P. T., & Gronenborn, A. M. (1990a) *Biochemistry 29*, 7387−7401.
Clore, G. M., Szabo, A., Bax, A., Kay, L. E., Driscoll, P. C., & Gronenborn, A. M. (1990b) *J. Am. Chem. Soc. 112*, 4989−4991.
Davis, D. G., & Bax, A. (1985) *J. Am. Chem. Soc. 107*, 2821−2822.
de la Torre, J. G., Navarro, S., Martinez, M. C. L., Diaz, F. G., & Cascales, J. J. L. (1994) *Biophys. J. 67*, 530−531.
Dickson, R., Larsen, B., Viitanen, P. V., Tormey, M. B., Geske, J., Strange, R., & Bemis, L. T. (1994) *J. Biol. Chem. 269*, 26858−26864.
Dubaquié, Y.; Looser, R., & Rospert, S. (1997) *Proc. Natl. Acad. Sci. U.S.A.* (in press).
Dyson, H. J., & Wright, P. E. (1991) *Annu. Rev. Biophys. Biophys. Chem. 20*, 519−538.
Farrow, N. A., Zhang, O. W., Forman-Kay, J. D., & Kay, L. E. (1995a) *Biochemistry 34*, 868−878.
Farrow, N. A., Zhang, O., Szabo, A., Torchia, D. A., & Kay, L. E. (1995b) *J. Biomol. NMR 6*, 153−162.
Farrow, N. A., Zhang, O. W., Forman-Kay, J. D., & Kay, L. E. (1997) *Biochemistry 36*, 2390−2402.
Fossati, G., Lucietto, P., Giuliani, P., Coates, A. R., Harding, S., Colfen, H., Legname, G., Chan, E., Zaliani, A., & Mascagni, P. (1995) *J. Biol. Chem. 270*, 26159−26167.
Freund, C., Ross, A., Plückthun, A., & Holak, T. A. (1994) *Biochemistry 33*, 3296−3303.
Goloubinoff, P., Diamant, S., Weiss, C., & Azem, A. (1997) *FEBS Lett. 407*, 215−219.
Gronenborn, A. M., Bax, A., Wingfield, P. T., & Clore, G. M. (1989) *FEBS Lett. 243*, 93−98.
Hansen, A. P., Petros, A. M., Meadows, R. P., & Fesik, S. W. (1994) *Biochemistry 33*, 15418−15424.
Hartl, F. U. (1996) *Nature 381*, 571−580.
Hendrix, R. W. (1979) *J. Mol. Biol. 129*, 375−392.
Hohfeld, J., & Hartl, F. U. (1994) *J. Cell Biol. 126*, 305−315.
Hohn, T., Hohn, B., Engel, A., & Wurtz, M. (1979) *J. Mol. Biol. 129*, 359−373.
Hunt, J. F., Weaver, A. J., Landry, S. J., Gierasch, L. M., & Deisenhofer, J. (1996) *Nature 379*, 37−45.
Hunt, J. F., van der Vies, S. M., Henry, L., & Deisenhofer, J. (1997) *Cell* (in press).
Ishima, R., & Nagayama, K. (1995) *Biochemistry 34*, 3162−3171.
Jeener, J., Meier, B. H., Bachmann, P., & Ernst, R. R. (1979) *J. Chem. Phys. 71*, 4546−4553.
Kay, L. E., Torchia, D. A., & Bax, A. (1989) *Biochemistry 28*, 8972−8979.
Koonin, E. V., & van der Vies, S. M. (1995) *Trends Biochem. Sci. 20*, 14−15.
Kraulis, P. J. (1991) *J. Appl. Crystallogr. 24*, 946−950.
Landry, S. J., & Gierasch, L. M. (1994) *Annu. Rev. Biophys. Biomol. Struct. 23*, 645−669.
Landry, S. J., Zeilstra-Ryalls, J., Fayet, O., Georgopoulos, C., & Gierasch, L. M. (1993) *Nature 364*, 255−258.
Landry, S. J., Taher, A., Georgopoulos, C., & van der Vies, S. M. (1996) *Proc. Natl. Acad. Sci. U.S.A. 93*, 11622−11627.
Langer, T., Pfeifer, G., Martin, J., Baumeister, W., & Hartl, F. U. (1992) *EMBO J. 11*, 4757−4765.
Lipari, G., & Szabo, A. (1982a) *J. Am. Chem. Soc. 104*, 4546−4559.
Lipari, G., & Szabo, A. (1982b) *J. Am. Chem. Soc. 104*, 4559−4570.
Logan, T. M., Theriault, Y., & Fesik, S. W. (1994) *J. Mol. Biol. 236*, 637−648.
Macura, S., Huang, Y., Suter, D., & Ernst, R. R. (1981) *J. Magn. Reson. 43*, 259−281.
Mande, S. C., Mehra, V., Bloom, B. R., & Hol, W. G. (1996) *Science 271*, 203−207.
Mandel, A. M., Akke, M., & Palmer, A. G., III (1996) *Biochemistry 35*, 16009−16023.
Marion, D., Ikura, M., & Bax, A. (1989) *J. Magn. Reson. 84*, 425−430.
Markus, M. A., Hinck, A. P., Huang, S., Draper, D. E., & Torchia, D. A. (1997) *Nat. Struct. Biol. 4*, 70−77.
McMullin, T. W., & Hallberg, R. L. (1988) *Mol. Cell. Biol. 8*, 371−380.
Messerle, B. A., Wider, G., Otting, G., Weber, C., & Wüthrich, K. (1989) *J. Magn. Reson. 85*, 608−613.
Monzini, N., Legname, G., Marcucci, F., Gromo, G., & Modena, D. (1994) *Biochim. Biophys. Acta 1218*, 478−480.
Nicholson, L. K., Yamazaki, T., Torchia, D. A., Grzesiek, S., Bax, A., Stahl, S. J., Kaufman, J. D., Wingfield, P. T., Lam, P. Y. S., Jadhav, P. K., Hodge, C. N., Domaille, P. J., & Chang, C. H. (1995) *Nat. Struct. Biol. 2*, 274−280.
Norwood, T. J., Boyd, J., Heritage, J. E., Soffe, N., & Campbell, I. D. (1990) *J. Magn. Reson. 87*, 488−501.
Nowak, U. K., Li, X., Teuten, A. J., Smith, R. A. G., & Dobson, C. M. (1993) *Biochemistry 32*, 298−309.
Palmer, A. G., Rance, M., & Wright, P. E. (1991) *J. Am. Chem. Soc. 113*, 4371−4380.
Palmer, A. G., III, Skelton, N. J., Chazin, W. J., Wright, P. E., & Rance, M. (1992) *Mol. Phys. 75*, 699−711.
Peng, J. W., & Wagner, G. (1992) *Biochemistry 31*, 8571−8586.
Pushkin, A. V., Tsuprun, V. L., Solovjeva, N. A., Shubin, V. V., Evstigneeva, Z. G., & Kretovich, W. L. (1982) *Biochim. Biophys. Acta 704*, 379−384.
Plateau, P., & Gueron, M. (1982) *J. Am. Chem. Soc. 104*, 7310−7311.
Redfield, C., Boyd, J., Smith, L. J., Smith, R. A. G., & Dobson, C. M. (1992) *Biochem. 31*, 10431−10437.
Redfield, C., Smith, R. A. G., & Dobson, C. M. (1994) *Nat. Struct. Biol. 1*, 23−29.

Roseman, A. M., Chen, S. X., White, H., Braig, K., & Saibil, H. R. (1996) *Cell 87*, 241−251.
Rospert, S., Junne, T., Glick, B. S., & Schatz, G. (1993) *FEBS Lett. 335*, 358−360.
Ryan, M. T., Naylor, D. J., Hoogenraad, N. J., & Høj, P. B. (1995) *J. Biol. Chem. 270*, 22037−22043.
Schmidt, M., Rutkat, K., Rachel, R., Pfeifer, G., Jaenicke, R., Viitanen, P., Lorimer, G., & Buchner, J. (1994) *Science 265*, 656−659.
Shaka, A. J., Lee, C. J., & Pines, A. (1988) *J. Magn. Reson. 77*, 274−293.
Sklenar, A. J., Lee, C. J., & Pines, A. (1987) *J. Magn. Reson. 74*, 469−479.
Sorensen, M. D., Kristensen, S. M., & Led, J. J. (1995) *J. Magn. Reson. 107*, 83−87.
Török, Z., Vigh, L., & Goloubinoff, P. (1996) *J. Biol. Chem. 271*, 16180−16186.
Torchia, D. A., Lyerla, J. R., Jr., & Quattrone, A. J. (1975) *Biochemistry 14*, 887−899.
van Mierlo, C. P. M., Darby, N. J., Keeler, J., Neuhaus, D., & Creighton, T. E. (1993) *J. Mol. Biol. 229*, 1125−1146.
Viitanen, P. V., Lorimer, G. H., Seetharam, R., Gupta, R. S., Oppenheim, J., Thomas, J. O., & Cowan, N. J. (1992) *J. Biol. Chem. 267*, 695−698.
Weissman, J. S., Hohl, C. M., Kovalenko, O., Kashi, Y., Chen, S. X., Braig, K., Saibil, H. R., Fenton, W. A., & Horwich, A. L. (1995) *Cell 83*, 577−587.
Wishart, D. S., Sykes, B. D., & Richards, F. M. (1992) *Biochemistry 31*, 1647−1651.
Wishart, D. S., Bigam, C. G., Holm, A., Hodges, R. S., & Sykes, B. D. (1995) *J. Biomol. NMR 5*, 67−81.
Zeilstra-Ryalls, J., Fayet, O., & Georgopoulos, C. (1991) *Annu. Rev. Microbiol. 45*, 301−325.
Zhang, O., & Forman-Kay, J. D. (1995) *Biochemistry 34*, 6784−6794.
Zhou, H., McEvoy, M. M., Lowry, D. F., Swanson, R. V., Simon, M. I., & Dahlquist, F. W. (1996) *Biochemistry 35*, 433−443.
Zink, T., Ross, A., Luers, K., Cieslar, C., Rudolph, R., & Holak, T. A. (1994) *Biochemistry 33*, 8453−8463.
Zondlo, J., Fisher, K. E., Lin, Z. L., Ducote, K. R., & Eisenstein, E. (1995) *Biochemistry 34*, 10334−10339.
Zuiderweg, E. R. P. (1990) *J. Magn. Reson., Ser. B 86*, 346−357.

BI971141P